Plasmonic effects in excitonic population transfer in a driven semiconductor–metal nanoparticle hybrid system

M. A. Antón,* F. Carreño, Sonia Melle, Oscar G. Calderón, and E. Cabrera-Granado
[1]*Escuela Universitaria de Óptica, Universidad Complutense de Madrid, C/ Arcos de Jalón 118, 28037 Madrid, Spain*

Joel Cox and Mahi R. Singh
[2]*Department of Physics and Astronomy, The University of Western Ontario, London, Canada N6A 3K7*
(Received 25 June 2012; published 5 October 2012)

We have investigated the coherent transfer of excitonic populations in a semiconductor quantum dot (SQD) modulated by the surface plasmon of a metallic nanoparticle (MNP). The SQD is considered as a three-level V-type atomic system. We applied a transform-limited laser pulse field resonant with the upper atomic levels of the SQD. When the SQD is close enough to the MNP, the otherwise equally populated atomic levels can be selectively excited. Selectivity population can be achieved by two physical mechanisms: an enhancement of the Rabi frequencies that drive the optical transitions, which depends on the polarization arrangement, and a frequency shift of the optical transitions that leads to a dynamical detuning.

DOI: 10.1103/PhysRevB.86.155305 PACS number(s): 78.67.−n

I. INTRODUCTION

Coherent optical control over individual quantum systems in semiconductors has been the subject of active research over the past decade[1] because of its potential applications in atom optics,[2] preparation of entanglement,[3] and quantum computation.[4,5] It also plays a central role in controlling chemical reaction dynamics.[6] Three main strategies, that is, temporal coherent control, optimal control, and adiabatic passage, have been proposed to realize quantum coherent control.[7] Stimulated Raman adiabatic passage (STIRAP)[1,8,9] has emerged as a very efficient and robust way to achieve complete coherent population transfer between two discrete states in an atomic or a molecular system. This technique has played a major role in population transfer in Λ and ladder systems.[1,10] There, complete population transfer from the initial state to the target state without populating the intermediate state could be achieved by applying time-delayed but partially overlapped pump and Stokes pulses in a counterintuitive order while the two-photon resonance and adiabatic conditions are fulfilled. An alternative technique for population transfer is Raman chirped adiabatic passage.[11–13] In this technique, chirped lasers with time-dependent frequencies are used to sweep through either one- or two-photon resonances in ladder and Λ systems, which results in efficient population transfer. Very recently, robust quantum dot exciton generation via STIRAP with frequency-swept optical pulses has been experimentally reported.[14] It should be noted that selectivity cannot be realized with a transform-limited pulse in the single-atom regime. However, Netz *et al*. have shown that selectivity in a V-type three-level system can be obtained by an applied field with a large linear chirped rate and a proper direction of the chirp.[15] Apart from one of the above-mentioned methods, it has been shown that in dense atomic media, near dipole-dipole interactions can cause a dynamic frequency chirp in the system. In particular, Crenshaw and Bowden showed that a dense two-level medium can be adiabatically inverted by the so-called intrinsic self-chirping.[16]

It is well known that dipole-dipole interactions occur naturally in nanometer-scale hybrid heterostructures. Nanometer-scale metallic structures have attracted plenty of attention because they can dramatically modify the optical properties of various optically active objects of similar dimensions, such as atoms, molecules, or semiconductor quantum dots. The interest in combining metal and semiconductor nanostructures stems from their complementary optical properties. When combined into heterostructures, the nanometer-scale vicinity of the two material systems leads to interactions between quantum-confined electronic states in semiconductor nanostructures and dielectric-confined electromagnetic modes in the metal counterpart. Such exciton-plasmon interactions allow the tailoring of absorption and emission properties, control of nanoscale energy-transfer processes, creation of new excitations in the strong-coupling regime, and the enhancement of optical nonlinearities.[17,18] Many interesting phenomena have been found in these coupled nanocrystals, such as the nonlinear Fano effect,[18] Förster energy transfer,[19] and local field enhancement.[20,21]

In the presence of an external laser field, the surface plasmon oscillation in metallic nanoparticles (MNPs) renormalizes the external field and enhances the electric field in the semiconductor quantum dots (SQDs). The strong modifications are conceptually well understood as a product of free-electron oscillations in the metal that induce strong localized electric fields near the surface of nanostructured metals. The large fields and the high confinement associated with the plasmonic resonances supported by these systems enable strong interactions with other photonic elements such as quantum emitters.[18,22,23] Significant attention has been focused on the emerging field of quantum plasmonics with the goal of making devices for quantum information processing[24,25] as single-photon transistors[26] or lasers.[27] Additionally, the possibility of reaching the quantum regime using plasmonic systems has also been addressed.[28–30] As a requisite for this goal, a lot of effort has been devoted to achieve coherent coupling between plasmons and a quantum emitter made of a solid-state qubit such as, for instance, a quantum dot, a single nitrogen vacancy center, or a single molecule, among others. When SQDs are placed in close proximity to a MNP,

exciton-plasmon coupling can lead to a dramatic change in the optical properties. This includes enhancement or suppression of their emission,[31] shift and broadening of their excitonic transitions,[31,32] enhancement of the Rabi flopping,[33] and optical bistability.[34] The broadening of excitonic transitions is related to Förster energy transfer from SQDs to MNPs, which is ultimately dissipated in the form of heat. Previous studies have shown that in SQD-MNP hybrid systems, the energy dissipation rate in the MNPs can be altered significantly.[23] For a system consisting of one pair of SQDs and a MNP, in particular, these studies have indicated that interference effects in the MNP can produce characteristic Fano-type asymmetric features in its energy absorption rate.[18,23] However, local field effects in the dynamics of exciton populations in SQD-MNP hybrid systems have received less attention. The dynamics of exciton populations in a V-type SQD close to a metallic nanorod has been considered previously in Ref. 35. In the case of an isolated SQD, it is well known that a transform-limited laser pulse with carrier frequency between the two upper levels excites these two states equally, i.e., it does not produce selective population of one of the upper levels. The aim of this paper is to investigate the role of exciton-plasmon effects on excitonic population transfer when an ultrashort pulse interacts with such a hybrid system. Here, we will show that the local field effects induced by exciton-plasmon interactions allow selective excitation of the excited excitonic states.

The paper is organized as follows: Section II establishes the model, i.e., the Hamiltonian of the system and the time-evolution equations of the atomic operators assuming the rotating wave approximation. Section III deals with the numerical simulations and discusses the possibility of optical selectivity of excitonic populations via plasmonic-induced self-chirping. Section IV summarizes the main conclusions.

II. THEORETICAL MODEL

We investigate quantum coherence and interference phenomena in a SQD-MNP hybrid system. We consider a spherical MNP with radius a coupled to a spherical SQD (Fig. 1). The center-to-center distance between the SQD and the MNP is denoted as R. For the description of the MNP, we use classical electrodynamics and the quasistatic approach. We consider a SQD in which the anisotropic electron-hole exchange interaction leads to the exciton state of the SQD splitting into two orthogonal polarization eigenstates. This allows us to model the system as a three-level V-type system. The three excitonic states are denoted as $|1\rangle$, $|2\rangle$, and $|3\rangle$, with energies $\hbar\omega_j$ ($j = 1$–3). The two single-excitonic transitions $|1\rangle \leftrightarrow |2\rangle$ and $|1\rangle \leftrightarrow |3\rangle$ are orthogonal linearly polarized[36] or left and right circularly polarized.[37] The resonant frequencies between the upper levels $|2\rangle$ and $|3\rangle$ and the ground level $|1\rangle$ are ω_{21} and ω_{31}, respectively. Note that $\omega_{31} - \omega_{21} = \omega_{32} \equiv 2\Delta$, ω_{32} being the frequency separation of the excited levels.

A laser field $\vec{E}$ with frequency ω_L couples the ground level $|1\rangle$ and the two upper levels $|2\rangle$ and $|3\rangle$, and is given by

$$\vec{E} = \tfrac{1}{2}[E_2(t)\vec{u}_2 + E_3(t)\vec{u}_3]e^{-i\omega_L t} + \text{c.c.}, \tag{1}$$

where E_2 (E_3) is the slowly varying amplitude along the $\vec{u}_2$ ($\vec{u}_3$) direction, which corresponds to the polarization of the transition $|1\rangle \leftrightarrow |2\rangle$ ($|1\rangle \leftrightarrow |3\rangle$). The laser frequency is set to the middle between the two resonances, i.e., $\omega_L = (\omega_{21} + \omega_{31})/2$.

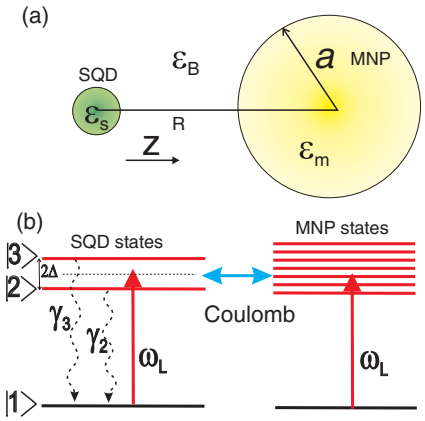

FIG. 1. (Color online) (a) The SQD-MNP hybrid system. The MNP has a radius a and a dielectric constant ϵ_m. The dielectric constants of the SQD and the environment are ϵ_s and ϵ_B, respectively. (b) Atomic states of the SQD and the MNP. The upper level decays to the ground level are denoted as γ_2 and γ_3.

The radius a of the MNP is on the nanometer scale. As the radius of the SQD is usually very small, it can be considered as a sphere with pointlike dipoles induced by the external field. The oscillating electric field created by the laser will generate plasmon oscillations in the MNP and electric dipoles in the SQD, which interact with each other via the dipole-dipole interaction and renormalize the external electric field. The original external field is assumed to be spatially uniform for the relatively small dimension of the hybrid system, and the quasistatic approximation is used. The dielectric function of the SQD is denoted as ϵ_s, while that of the host medium is denoted as ϵ_B (see Fig. 1). The dielectric function of the MNP is $\epsilon_m(\omega)$, which we take in a renormalized Drude approximation:

$$\epsilon_m(\omega) = \epsilon_\infty - \frac{\omega_p^2}{\omega^2 + i\gamma_p\omega}, \tag{2}$$

where ϵ_∞ is the high-frequency limit of the metal dielectric function, ω_p is the bulk plasmon frequency, and γ_p is the Landau damping constant.

The Hamiltonian of the hybrid system can be expressed as

$$H = H_0 + H_E + V_B + \mathfrak{L}\rho, \tag{3}$$

where

$$\begin{aligned} H_0 &= \hbar\sum_{j=1}^{3}\omega_j\hat{\sigma}_{jj} + \hbar\sum_{nk}\omega_{nk}p_{nk}^{+}p_{nk}, \\ H_E &= -\frac{1}{2}\sum_{j=2}^{3}\mu_{j1}E_{\text{SQD}}^{(j)}e^{-i\omega_L t}\hat{\sigma}_{j1} + \text{H.c.}, \\ V_B &= \hbar\sum_{j=2}^{3}\sum_{nk}\left(g_{j1}^{(0)} + g_{j1}^{(d)}\right)p_{nk}\hat{\sigma}_{j1}e^{-i\omega_{nk}t} + \text{H.c.}, \end{aligned} \tag{4}$$

$\mathfrak{L}\rho$ is the Liouvillian of the system, and H.c. stands for the Hermitian conjugate. The field-matter coupling constant for the vacuum modes is $g_{j1}^{(0)}$, whereas $g_{j1}^{(d)}$ is the coupling constant for the polaritonic modes. Here p_{nk} is the annihilation operator

of the nkth mode of the polaritonic field with angular frequency ω_{nk}. The parameters μ_{j1}, with $j = 2$ and 3, are the interband dipole matrix elements of the excitonic transitions $|2\rangle \rightarrow |1\rangle$ and $|3\rangle \rightarrow |1\rangle$, respectively. $E^{(j)}_{\mathrm{SDQ}}$ $(j = 2,3)$ is the slowly varying amplitude of the total field felt by the SQD polarized along the $|1\rangle \leftrightarrow |j\rangle$ transition, which is given by

$$E^{(j)}_{\mathrm{SQD}} = \frac{1}{\epsilon_{\mathrm{effs}}}\left[E_j + \frac{1}{4\pi\epsilon_0\epsilon_B}\frac{S_j P^{(j)}_{\mathrm{MNP}}}{R^3}\right], \tag{5}$$

where $\epsilon_{\mathrm{effs}} = (2\epsilon_B + \epsilon_s)/3\epsilon_B$, and S_j is 2 or -1 when the electric field E_j is polarized along the axis of the hybrid system or in the orthogonal direction. The z direction corresponds to the axis of the hybrid system (see Fig. 1). The dipole $P^{(j)}_{\mathrm{MNP}}$ $(j = 2,3)$ comes from the charge induced on the surface of the MNP, and depends on the total field due to the SQD[37] as

$$P^{(j)}_{\mathrm{MNP}} = 4\pi\epsilon_0\epsilon_B a^3\gamma(\omega)E^{(j)}_{\mathrm{MNP}}, \tag{6}$$

where $E^{(j)}_{\mathrm{MNP}}$ $(j = 2,3)$ is the slowly varying field amplitude at frequency ω_L felt by the MNP, which is given by

$$E^{(j)}_{\mathrm{MNP}} = E_j + \frac{1}{4\pi\epsilon_0\epsilon_B}\frac{S_j P^{(j)}_{\mathrm{SQD}}}{R^3}, \tag{7}$$

and $\gamma(\omega) = [\epsilon_m(\omega) - \epsilon_B]\,/\,[2\epsilon_B + \epsilon_m(\omega)]$ is the dipole polarizability of the MNP. The dipole $P^{(j)}_{\mathrm{SQD}}$ $(j = 2,3)$ is expressed via the off-diagonal elements of the density matrix as follows:

$$P^{(j)}_{\mathrm{SQD}} = \mu_{j1}\rho_{j1}. \tag{8}$$

In Eq. (7), we have not included the factor ϵ_{effs} to account for the screening of the SQD dipole field due to the SQD dielectric response, since the polarization $P^{(j)}_{\mathrm{SQD}}$ already contains this factor, as pointed out by Malyshev *et al.*[34]

Substituting Eqs. (7) and (8) back into Eq. (6), we obtain

$$P^{(j)}_{\mathrm{MNP}} = 2\pi\epsilon_0\epsilon_B a^3\gamma(\omega)\left(E_j + \frac{1}{2\pi\epsilon_0\epsilon_B}\frac{S_j\mu_{j1}\rho_{j1}}{R^3}\right). \tag{9}$$

Finally, the slowly varying amplitudes of the fields in the SQD are

$$E^{(j)}_{\mathrm{SQD}} = \frac{E_j}{\epsilon_{\mathrm{effs}}}\left(1 + \frac{S_j a^3\gamma(\omega)}{R^3}\right) + \frac{a^3\gamma(\omega)S_j^2\mu_{j1}\rho_{j1}}{2\pi\epsilon_0\epsilon_B\epsilon_{\mathrm{effs}}R^6}. \tag{10}$$

By introducing Eq. (10) into Eq. (4), the total Hamiltonian of the SQD in the dipole approximation may be expressed as follows:

$$\begin{aligned}
H_0 &= \hbar\sum_{j=1}^{3}\omega_j\hat{\sigma}_{jj},\\
H_E &= -\hbar\sum_{j=2}^{3}(\Omega_j + G_j\rho_{j1})\hat{\sigma}_{j1}e^{-i(\omega_L-\omega_{j1})t} + \mathrm{H.c.},\\
V_B &= \hbar\sum_{j=2}^{3}\sum_{nk}\left(g^{(0)}_{j1} + g^{(d)}_{j1}\right)p_{nk}\hat{\sigma}_{j1}e^{-i(\omega_{nk}-\omega_{j1})t} + \mathrm{H.c.},
\end{aligned} \tag{11}$$

where we have introduced the magnitudes Ω_j and G_j $(j = 2,3)$, which contain the effects of both coupling fields and plasmons, and are explicitly given by

$$\begin{aligned}
\Omega^0_j &= \frac{\mu_{j1}E_j}{2\hbar\epsilon_{\mathrm{effs}}},\\
\Omega_j &= \Omega^0_j\left[1 + \frac{S_j a^3\gamma(\omega)}{R^3}\right],\\
G_j &= \frac{S_j^2\mu_{j1}^2 a^3\gamma(\omega)}{4\pi\epsilon_0\epsilon_B\hbar\epsilon_{\mathrm{effs}}R^6}.
\end{aligned} \tag{12}$$

In the above equations, Ω_j is the normalized Rabi frequency associated with the external field and the field produced by the induced dipole moment P_{MNP} of the MNP. In addition, G_j shows the interaction between the polarized SQD and the MNP. Note that G_j is a complex quantity. When the laser field is weak, the imaginary part of G_j represents the Förster energy transfer rate from the SQD to the MNP and therefore contributes to the damping rate of the SQD. The real part of G_j refers to the redshift of the SQD transition caused by the plasmonic effects.[23,33] It should be noted that the excitation with circularly polarized fields would manifest as an overall extra phase factor of $\pi/2$ affecting only one of the Rabi frequencies, whereas the G_j factors remain unaltered. The phase factor has no influence on the dynamics of the system, thus this kind of excitation would produce the same result as the one obtained with the simultaneous excitation with linearly polarized fields in the current system. However, the use of an external magnetic field would modify the behavior of the system due to mixing of the states arising from the exchange between the heavy holes and the electron spins. This topic has been analyzed in detail in Ref. 37.

From Eq. (11), we obtain the following equations of motion for the density matrix elements of the SQD in the hybrid system and in an appropriated rotating frame:

$$\begin{aligned}
\frac{\partial\rho_{31}}{\partial t} &= -\left\{\frac{\gamma_3}{2} + i\left[\Delta - G_3(\rho_{11}-\rho_{33})\right]\right\}\rho_{31}\\
&\quad + i\Omega_3(\rho_{11}-\rho_{33}) - i(\Omega_2 + G_2\rho_{21})\rho_{32},\\
\frac{\partial\rho_{21}}{\partial t} &= -\left\{\frac{\gamma_2}{2} - i\left[\Delta + G_2(\rho_{11}-\rho_{22})\right]\right\}\rho_{21}\\
&\quad + i\Omega_2(\rho_{11}-\rho_{22}) - i(\Omega_3 + G_3\rho_{31})\rho_{23},\\
\frac{\partial\rho_{32}}{\partial t} &= -\left[\frac{\gamma_2+\gamma_3}{2} + 2i\Delta\right]\rho_{32} + i(\Omega_3 + G_3\rho_{31})\rho_{12}\\
&\quad - i(\Omega_2^* + G_2^*\rho_{12})\rho_{31},\\
\frac{\partial\rho_{33}}{\partial t} &= -\gamma_3\rho_{33} + i(\Omega_3 + G_3\rho_{31})\rho_{13} - i(\Omega_3^* + G_3^*\rho_{13})\rho_{31},\\
\frac{\partial\rho_{22}}{\partial t} &= -\gamma_2\rho_{22} + i(\Omega_2 + G_2\rho_{21})\rho_{12} - i(\Omega_2^* + G_2^*\rho_{12})\rho_{21}.
\end{aligned} \tag{13}$$

Here γ_j with $j = 2,3$ represents the radiative decay rates of the excitonic states $|j\rangle$ due to spontaneous emission.

A close inspection of Eq. (13) reveals that the plasmonic interaction manifests in two ways: the first one relies on the enhancement of the Rabi frequencies which drive the SQD according to the values given in Eq. (12). A different enhancement of the Rabi frequency experienced by the two transitions arises from the polarization arrangement (S_j). The second mechanism can be formally interpreted as a nonlinear frequency shift in the optical resonance causing a dynamical

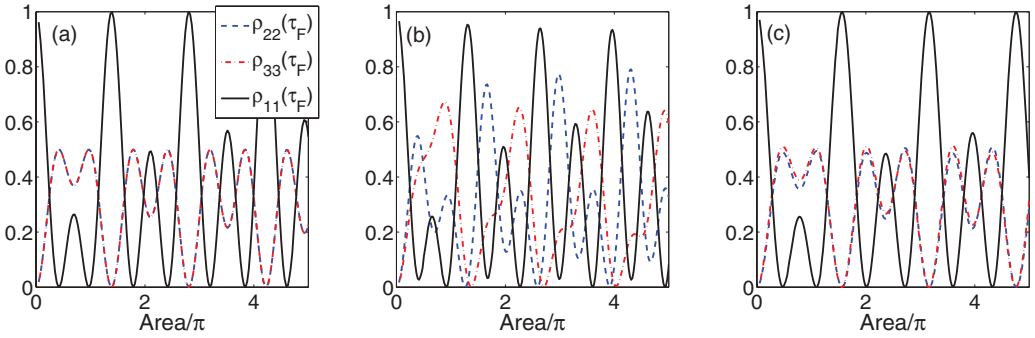

FIG. 2. (Color online) The final populations of the SQD levels as a function of the pulse area (Ω_0) in multiples of π. (a) Without a MNP. (b), (c) With a MNP at a distance $R = 10$ nm and different polarization parameters: (b) $S_2 = 2$, $S_3 = -1$; (c) $S_2 = -1$, $S_3 = -1$.

detuning. The values of the dynamical detuning for the optical coherences ρ_{31} and ρ_{21} are given by $\mathrm{Re}(G_3)(\rho_{11} - \rho_{33})$ and $\mathrm{Re}(G_2)(\rho_{11} - \rho_{22})$, respectively. The two above-mentioned mechanisms depend strongly on the SQD-MNP distance R. We address the issue of selective population transfer in Sec. III by means of numerical simulations for two different hybrid systems where these two regimes can be achieved.

III. NUMERICAL SIMULATIONS AND DISCUSSION

The strength of the plasmon-exciton interaction G_j is proportional to the square of the dipolar moment, whereas the renormalization factor of the Rabi frequency does not depend on the dipolar moment [see Eq. (12)]. An appropriate selection of SQDs with a remarkable difference between their dipolar moments will allow us to isolate the two regimes of operation of the hybrid system. We consider a spherical gold MNP with radius $a = 6$ nm, plasma frequency $\hbar\omega_p = 8.54$ eV, high-frequency limit $\epsilon_\infty = 9.54$, and damping constant $\hbar\gamma_p = 0.066$ eV. With these parameters, the Drude model assumed in Eq. (2) provides a reasonably good fit to tabulated experimental data for photon energies smaller than 3 eV.[38] We also consider that the dielectric constant of the host material is $\epsilon_B = 2.25$, which corresponds to silica. We also consider that the system interacts with a Gaussian pulse given by $\Omega_2^0(\tau) = \Omega_3^0(\tau) = \frac{\Omega_0}{\sqrt{2\pi\sigma^2}} e^{-(\tau-\tau_p)^2/2}$, where $\sqrt{2}\sigma$ is the $1/e$ half-width, Ω_0 is a normalized (dimensionless) peak amplitude which measures the pulse area, τ_p is the center of the pulse, and $\tau = t/\sigma$ is the normalized time variable. We consider a pulse bandwidth large enough to be able to excite both upper levels; in particular, we take $\sigma = 1/\omega_{32}$. The previous definition for the Rabi frequency allows us to specify the pulse area by simply selecting the magnitude of Ω_0. We have carried out numerical simulations by solving the density matrix equations (13), using a time interval ranging from $\tau_0 = 0$ to $\tau_F = 40$. This time interval allows us to neglect dissipation effects and guarantees that a steady state is reached.

A. Regime of low dynamical detuning and asymmetric field enhancement

To analyze this regime, we consider a single self-assembled $In_{0.5}Ga_{0.5}As/GaAs$ SQD,[39] where the fine-structure split states $|2\rangle$ and $|3\rangle$ of an exciton define a V-type three-level system composed of two orthogonal transition dipole moments. These states originate in the shape anisotropy of the SQD[40] and play an important role in Rabi oscillations[41] and Raman beats.[42] We use the following parameters to describe this particular SDQ: $\epsilon_s = 12.96$, $\hbar\omega_{21} = 1.38$ eV, an energy splitting of $\hbar\omega_{32} = 70\,\mu$eV, a relaxation time of $\gamma_2 \simeq \gamma_3 = 1.25\ \mathrm{ns}^{-1}$, and dipole moments $\mu_{21} = 22$ D and $\mu_{31} = 17$ D (see Ref. 38). The temporal pulse length is $\sigma \simeq 9.4$ ps.

We analyze the influence of the pulse area (Ω_0) on the population of the upper levels. Figure 2(a) displays the distribution of the populations among the different levels for an isolated SQD: there we appreciate that the upper levels are equally populated regardless of the pulse area, thus no selectivity is achieved for the band-limited pulse. This is an expected result since the spectral width of the incident pulse is wider than the energy splitting between the excited states, and the pulse has a carrier frequency at resonance with the center of the splitting. However, this behavior is dramatically modified when we consider the joint system formed by the SQD and MNP, as depicted in Fig. 2(b), where the polarization parameters are $S_2 = 2$ and $S_3 = -1$. This polarization configuration means that the renormalization of the Rabi frequency is different for each transition. This leads the system to exhibit selective population transfer. The maximum transfer of population is achieved for a pulse area close to 5.63π, which corresponds to a peak intensity in the order of MW/cm^2. On the other hand, when a SQD is placed in such a way that the two optical transitions experience the same polarization parameter ($S_2 = S_3 = -1$), the two upper levels become nearly equally populated independent of the pulse area [see Fig. 2(c)]. In this case, the results obtained resemble those presented in Fig. 2(a) in the absence of a MNP. This result can be easily explained by taking into account the fact that the enhancement of the Rabi frequencies given in Eq. (12) is the same for both transitions. In conclusion, the asymmetric field enhancement induced by the polarization arrangement leads to population selectivity.

Now we turn our attention to the time dynamics of the system for various values of the separation distance R and for the polarization configuration considered in Fig. 2(b). We use a pulse area of $\Omega_0 = 5.63\pi$. We can appreciate in Fig. 3(a) that for a separation $R = 40$ nm, the populations after the pulse is off are very similar, so no selectivity occurs. For this separation distance, the enhancement factor of the Rabi frequency, which is proportional to $1/R^3$ as indicated in Eq. (12), is negligible. However, when the separation distance R decreases, selectivity is obtained as shown in Figs. 3(b)–3(d). In the case of $R =$

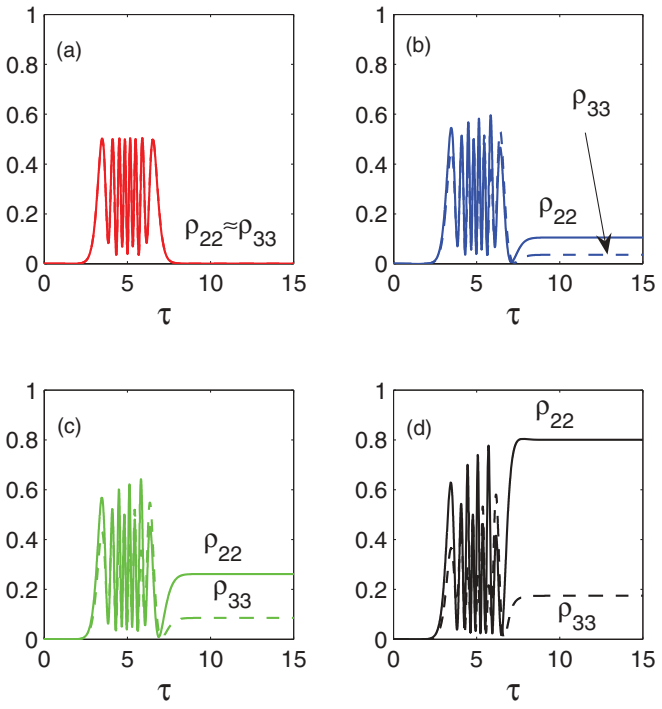

FIG. 3. (Color online) Time evolution of populations ρ_{22} (solid line) and ρ_{33} (dashed line) for a pulse area of $\Omega_0 = 5.63\pi$ and different MNP-SQD separations: (a) $R = 40$ nm; (b) $R = 15$ nm; (c) $R = 13$ nm; (d) $R = 10$ nm. Polarization parameters: $S_2 = 2$ and $S_3 = -1$.

10 nm, the dynamical frequency shift parameters are in the order of $G_3 \simeq 0.05\omega_{32}$ and $G_2 \simeq 0.33\omega_{32}$. Thus, the frequency shifts are negligible in comparison to the energy splitting ω_{32}, which means that the dynamical detuning phenomenon does not play a significant role.

The distribution of population in the upper levels as a function of the SQD to MNP distance is plotted in Fig. 4(a). Note that for the pulse area considered, $\Omega_0 = 5.63\pi$, the highest selectivity is achieved around $R \approx 10$ nm and the increase of the SQD-MNP distance results in a tendency toward the equalization of the upper levels' populations. The physical origin of this behavior relies on the fact that each transition experiences a different enhanced field whose ultimate origin arises from the difference of the two polarization parameters $S_2 = 2$ and $S_3 = -1$. This effect is clearly revealed in Fig. 4(b), where the dependence of the effective Rabi frequency versus distance is depicted. The asymptotic behavior indicates that at large distances, the two transitions are almost equally driven, thus no selectivity is produced.

Contour plots of the final population achieved in states $|2\rangle$ and $|3\rangle$ as a function of the pulse area (Ω_0) and the SQD-MNP separation (R) are depicted in Figs. 4(c) and 4(d), respectively. It can be seen that almost complete population transfer for either of the two upper levels can be obtained by suitably adjusting the pulse area and the distance R. Note that level $|3\rangle$ can be populated in a larger amount for a wider range of distances than level $|2\rangle$. In addition, it should be remarked that selectivity is absent for any pulse area when the distance R goes beyond 30 nm.

B. Regime of large dynamical detuning

To analyze the frequency shifts of the optical transitions leading to large dynamical detuning, we have considered another hybrid system formed by a single self-assembled GaAs/$Al_{0.3}Ga_{0.7}$As/GaAs SQD,[41] where the fine-structure split states $|2\rangle$ and $|3\rangle$ of an exciton defines also a V-type three-level system composed of two orthogonal transition dipole moments. In this system, the frequency shift can become larger than the splitting of upper states. The dipole moments of this SQD reach the values of $\mu_{21} \simeq \mu_{13} = 75$ D,[41,43] nearly three times greater than those considered in the previous SQD, thus the influence of the dynamical detuning terms will become more important, since the factors G_j scale with the square of the dipole moments. We also consider $\epsilon_s = 12.96$ for this SQD. Other parameters adapted to this system are $\hbar\omega_{21} = 1.6221$ eV and the energy splitting of $\hbar\omega_{32} = 10$ μeV. We set the polarization parameters $S_2 = 2$, $S_3 = -1$, and the temporal pulse length in the order of $\sigma \simeq 66$ ps.

The influence of the pulse area (Ω_0) on the population of the upper levels is displayed in Fig. 5. There we can appreciate that state $|3\rangle$ is preferentially populated for almost all the pulse areas considered. The reason for this behavior will be addressed below. It is worth mentioning that for certain values of the pulse area, the population of level $|2\rangle$

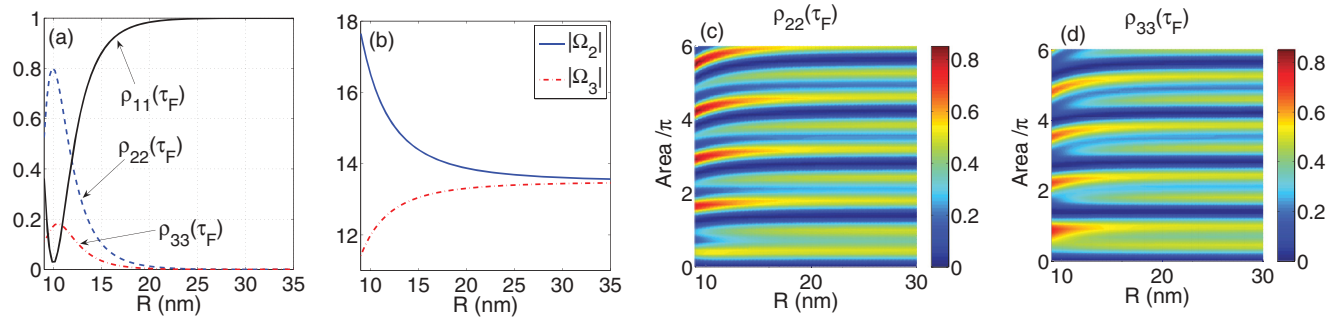

FIG. 4. (Color online) (a) Final population of the three levels $\rho_{11}(\tau_F)$ (solid line), $\rho_{22}(\tau_F)$ (dashed line), and $\rho_{33}(\tau_F)$ (dashed-dotted line) vs the MNP-SQD separation R for a pulse area of $\Omega_0 = 5.63\pi$. (b) Effective Rabi frequency for the two transitions vs R for a pulse area of $\Omega_0 = 5.63\pi$. (c), (d) Contour map of the final population transfer for $\rho_{22}(\tau_F)/\rho_{33}(\tau_F)$, for varying the pulse area Ω_0 and the separation distance R. The rest of the parameters are as in Fig. 2(b).

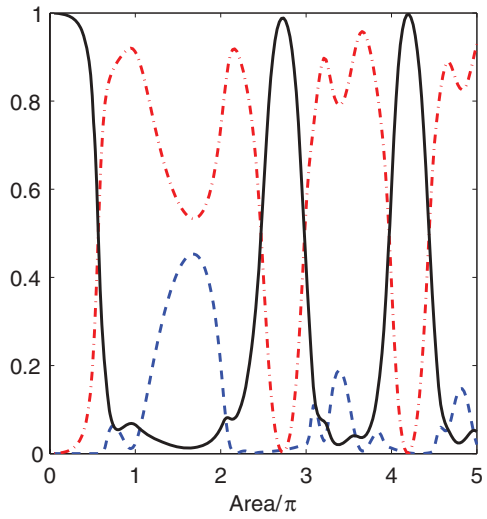

FIG. 5. (Color online) The final populations of the SQD levels as a function of the pulse area Ω_0 in multiples of π in the presence of the MNP at a distance $R = 11.7$ nm. Polarization parameters: $S_2 = 2$, $S_3 = -1$. $\rho_{11}(\tau_F)$ (solid line), $\rho_{22}(\tau_F)$ (dashed line), and $\rho_{33}(\tau_F)$ (dashed-dotted line).

is close to zero, which is of special interest to obtain a nearly complete inversion between levels $|3\rangle$ and $|1\rangle$. Once we have determined the influence of the pulse area on the redistribution of populations, let us consider the time dynamics of the hybrid system for several distances. To this end, we have plotted in Fig. 6 the upper level populations versus time for several distances and a fixed value of the pulse area $\Omega_0 = 0.4\pi$.

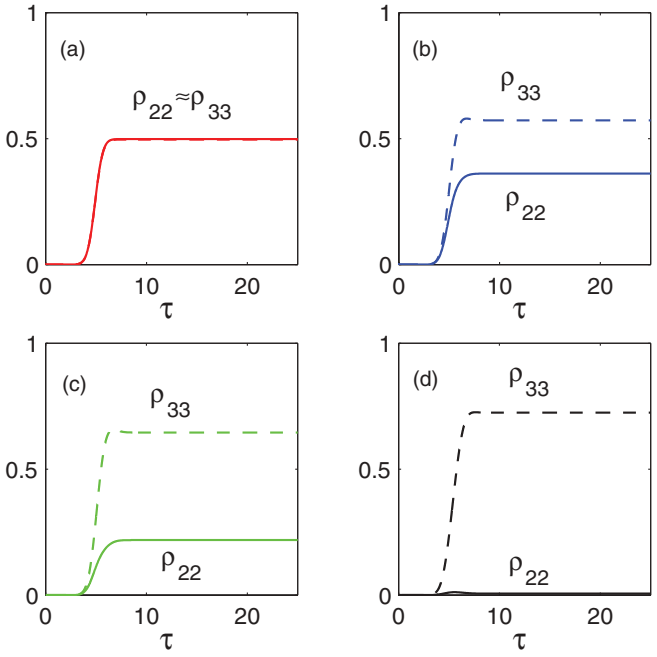

FIG. 6. (Color online) Time evolution of populations ρ_{22} (solid line) and ρ_{33} (dashed line) for a pulse area of $\Omega_0 = 0.4\pi$ and different MNP-SQD separations: (a) $R = 45$ nm; (b) $R = 17.5$ nm; (c) $R = 16$ nm; (d) $R = 12.8$ nm. Polarization parameters: $S_2 = 2$ and $S_3 = -1$.

The most interesting finding relies on the fact that even for a small area of the incident pulse, the population transfer to level $|3\rangle$ can be tuned by selecting the closeness of the SQD to the MNP. In particular, when the distance R approaches 12.8 nm, the transfer is very high. This result contrasts with the one obtained when considering the same situation for the other SQD [see Fig. 2(b)], where the upper levels' populations achieved for similar values of the parameters are very close to each other. This indicates that the effect of the dynamical detuning in the transfer of population results in a major selectivity. Similar asymmetric behavior originating from the local field correction in the nonlinear optical response of dense three-level systems in V-type[44] and Λ-type systems[45] has been found in the context of superradiant emission.

The numerical findings in this regime can be qualitatively explained on the basis of the following considerations. In the parameter space corresponding to the hybrid system considered in this subsection, the dipolar moments are so high that the interaction of the MNP with the SQD produces high values of the frequency-shift factors, G_2 and G_3, in comparison to the upper levels' splitting ω_{32}. In addition, G_2 will become different from G_3 due to the polarization parameters ($S_2 = 2$ and $S_3 = -1$), in fact, $|G_2| = 4|G_3|$. These two effects result in high and different sweeps of the effective detuning experienced by each optical transition. The most of-resonant transition will be almost decoupled and the population will transfer to the other upper state. This point is illustrated in Fig. 7(a), where the normalized dynamical detuning of both transitions, $\Delta_{12}^d = \sigma\,[-\Delta - \mathrm{Re}(G_2)(\rho_{11} - \rho_{22})]$ (solid line) and $\Delta_{13}^d = \sigma\,[\Delta - \mathrm{Re}(G_3)(\rho_{11} - \rho_{33})]$ (dashed line), versus time τ is displayed for the case considered in Fig. 6(d). The horizontal solid line is used as a guide to the eye to indicate the resonance condition. The dotted line is the input pulse and is also displayed to help interpret the time evolution of the dynamical detuning. It can be seen that the transition $|1\rangle \leftrightarrow |2\rangle$ is far detuned (solid line) in comparison to the transition $|1\rangle \leftrightarrow |3\rangle$ (dashed line) at the beginning of the interaction ($\tau \approx 0$). As the incident pulse evolves in time, transition $|1\rangle \leftrightarrow |3\rangle$ tends to resonance. When $\tau = 5$, which nearly coincides with the center of the pulse, this transition reaches resonance. However, at this time, the other transition remains of-resonance, and therefore level $|2\rangle$ will be populated to a lesser extent than level $|3\rangle$. This dynamical detuning can be interpreted as an intrinsic self-chirping, whose chirped rates are governed by the slopes of the initial part of $\mathrm{Re}(G_2)(\rho_{11} - \rho_{22})$ and $R(G_3)(\rho_{11} - \rho_{33})$, respectively. These two slopes (χ_{1j}, $j = 2,3$) have been numerically determined from Fig. 7(a) and used to solve Eq. (13) by substituting the dynamical detuning by the equivalent chirped rates in the optical detunings. That is, we make the replacement $-G_j(\rho_{11} - \rho_{jj}) \to \chi_{1j}\tau/\sigma$, and set to zero the other terms involving G_j, while keeping constant the rest of the parameters. This procedure will help us to evaluate whether the effect of chirping of the incident pulse could mimic the effect of dynamical detuning. The time evolution of the chirped detunings is shown with solid and dashed lines in Fig. 7(b). The inset represents the time evolution of populations obtained by solving the Bloch equations when the aforementioned replacement is carried out. We can devise that this substitution reproduces the essentials obtained in Fig. 6(d). Therefore, a dynamical frequency chirp induced by plasmon-

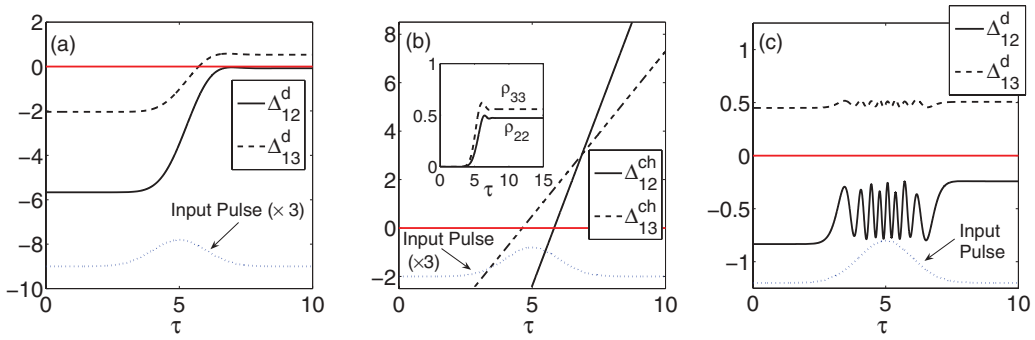

FIG. 7. (Color online) (a) Time evolution of the normalized dynamical detuning $\Delta_{12}^{d} = \sigma\,[-\Delta - \mathrm{Re}(G_2)(\rho_{11} - \rho_{22})]$ (solid line) and $\Delta_{13}^{d} = \sigma\,[\Delta - \mathrm{Re}(G_3)(\rho_{11} - \rho_{33})]$ (dashed line) for a pulse area of $\Omega_0 = 0.47\pi$ and $R = 12.8$ nm. Polarization parameters: $S_2 = 2$ and $S_3 = -1$. (b) Time evolution of the linear chirped detunings $\Delta_{12}^{\mathrm{ch}} = -\sigma\Delta + \chi_{12}\tau$ (solid line) and $\Delta_{13}^{\mathrm{ch}} = \sigma\Delta + \chi_{13}\tau$ (dashed line). The inset shows the time evolution of population ρ_{22} and ρ_{33}. Linear chirped rates are $\chi_{13} = 1.36$ and $\chi_{12} = 2.90$. (c) Time evolution of dynamical detuning Δ_{12}^{d} (solid line) and Δ_{13}^{d} (dashed line) for the case considered in Fig. 3(d). The dotted line is the input pulse magnified. The horizontal line indicates the resonance condition.

SQD interaction could explain the population selectivity. We have plotted for completeness in Fig. 7(c) the time evolution of the normalized dynamical detuning Δ_{12}^{d} (solid line) and Δ_{13}^{d} (dashed line) in the case of negligible dynamical detuning [$\mathrm{Re}(G_j) \ll \Delta$] considered in the preceding subsection [see Fig. 3(d)]. There we can appreciate that the effective detuning of the two optical transitions does not experience a significant change and stays close to their original values in the absence of dynamical detuning. In conclusion, the main physical reason for population selectivity in the SQD analyzed in this subsection is the dynamical shift of the excitonic resonance frequencies, which are represented by the nonlinear terms $G_2(\rho_{11} - \rho_{22})$ and $G_3(\rho_{11} - \rho_{33})$ in Eq. (13). These shifts break the symmetry of the field hybrid system interaction.

C. Multiple excitation pulses

One may wonder whether the application of a second pulse would allow us to purify the final state. To this end, we carried out numerical simulations by considering the successive application of two delayed pulses, i.e., the Rabi frequency of the fields reads

$$\Omega_j^0(\tau) = \frac{\Omega_0}{\sqrt{2\pi\sigma^2}}\left[e^{-(\tau-\tau_{p1})^2/2} + f_{2p}e^{-(\tau-\tau_{p2})^2/2}\right]. \quad (14)$$

This scheme is a simplified version of a technique that was recently considered in Ref. 46 for a Λ-type atom and in Ref. 47 for a double Λ-type atom. In both cases, the application of a train of pulse pairs resulted in an enhancement of the population transfer efficiency. In the present case, we fix the area of the first pulse and allow the second pulse to have an area equal to a fraction f_{2p} of the area of the first pulse, thus f_{2p} varies from 0 (absence of second pulse) to 1 (second pulse identical in area to the first one).

The application of two pulses is expected to improve the efficiency of population transfer in the case of low dynamical detuning, since in the other case the initial condition for the second pulse will find the system very far detuned. Thus we resort to considering in this subsection the SQD analyzed in Ref. 39.

Figure 8 displays the final populations reached for different peak amplitudes of the second pulse with respect to the first one. The two pulses are tuned to the middle of the upper doublet and share the same temporal width. The pulses are applied at times $\tau_{p1} = 5$ and $\tau_{p2} = 10$, respectively, and they overlap slightly in time. We can observe that the application of a second pulse allows us to manage the population redistribution of the two upper levels. Figure 8(a) displays the final populations of the two excited levels when the MNP is far from the SQD. This result indicates that the final values of the upper level's populations can be tuned by changing the area of the second pulse, however they are almost equally populated. When the MNP is close to the SQD, the dipole-dipole interaction results in one of the upper levels being preferentially populated. Figure 8(b) displays the final population reached for different peak amplitudes of the second pulse. Here we find that one of the upper levels can be depopulated, and a wide variety of coherent superpositions between each of the two upper states can be realized by suitably changing the amplitude of the second pulse. The upper level's populations can also be tuned by using different areas of the first pulse. The application of

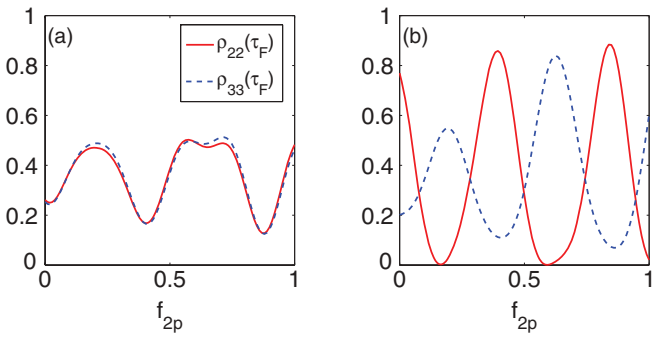

FIG. 8. (Color online) The final populations of the two excited levels of the SQD as a function of the peak value of the second pulse with respect to the first pulse. The first pulse is centered at time $\tau_{p1} = 5$ while the second one is centered at time $\tau_{p2} = 10$. The two pulses share the same width, and the area of the first pulse is $\Omega_0 = 3\pi$. The rest of the parameters are as in Fig. 2(b). (a) $R = 40$ nm; (b) $R = 10$ nm.

a train of pulses to the SQD-MNP hybrid system is currently under study and will be the subject of further consideration in a future work.

IV. CONCLUSIONS

In conclusion, we have investigated the population transfer in two different SQD-MNP hybrid systems interacting with a broadband pulse. Based on the numerical results obtained by solving the density matrix equations of motion, we demonstrate that a selective population of the excitonic states in a SQD can be achieved even with a transform-limited pulse. It is shown that by a proper selection of the distance between the SQD and the MNP and the pulse area, an arbitrary coherent superposition state can be created.

Two physical phenomena can lead the system to exhibit selective population transfer. First, plasmon-SDQ interaction produces a renormalization of the Rabi frequencies which drive the optical transitions. This renormalization is very different for both transitions due to the different polarization factors. Second, the strong plasmon interaction that occurs in SQDs with high values of the transition dipole moments leads to a decoupling of one of the transitions from the other due to the emergence of a large dynamical detuning. This last mechanism has been intuitively explained in terms of a dynamic frequency chirp induced by plasmon-SDQ interaction. We further studied the effects of considering multiple pulses to improve the efficiency of population transfer.

ACKNOWLEDGMENTS

The authors want to express their gratitude to the referees for their comments and suggestions, which helped us to improve the work. This work has been supported by Project No. FIS2010-22082 (MCINN) from Spain.

*antonm@fis.ucm.es

[1] K. Bergmann, H. Theuer, and B. W. Shore, Rev. Mod. Phys. **70**, 1003 (1998).
[2] M. Weitz, B. C. Young, and S. Chu, Phys. Rev. A **50**, 2438 (1994).
[3] A. S. Parkins, P. Marte, P. Zoller, O. Carnal, and H. J. Kimble, Phys. Rev. A **51**, 1578 (1995).
[4] T. Pellizzari, S. A. Gardiner, J. I. Cirac, and P. Zoller, Phys. Rev. Lett. **75**, 3788 (1995).
[5] C. Monroe, Nature (London) **416**, 238 (2002).
[6] P. Dittmann, F. P. Pesl, J. Martin, G. W. Coulston, G. Z. He, and K. Bergmann, J. Chem. Phys. **97**, 9472 (1992).
[7] P. Kral and M. Shapiro, Rev. Mod. Phys. **79**, 53 (2007).
[8] N. V. Vitanov, T. Halfmann, and B. W. Shore, Annu. Rev. Phys. Chem. **52**, 763 (2001).
[9] N. V. Vitanov, M. Fleischhauer, B. W. Shore, and K. Bergmann, Adv. At. Mol. Opt. Phys. **46**, 55 (2001).
[10] I. R. Sola and V. S. Malinovsky, Phys. Rev. A **68**, 013412 (2003).
[11] S. Chelkowski and G. N. Gibson, Phys. Rev. A **52**, R3417 (1995).
[12] B. Broers, H. B. van Linden van den Heuvell, and L. D. Noordam, Phys. Rev. Lett. **69**, 2062 (1992).
[13] J. S. Melinger, S. R. Gandhi, A. Hariharan, D. Goswami, and W. S. Warren, J. Chem. Phys. **101**, 6439 (1994).
[14] C. M. Simon, T. Belhadj, B. Chatel, T. Amand, P. Renucci, A. Lemaitre, O. Krebs, P. A. Dalgarno, R. J. Warburton, X. Marie, and B. Urbaszek, Phys. Rev. Lett. **106**, 166801 (2011).
[15] R. Netz, T. Feurer, G. Roberts, and R. Sauerbrey, Phys. Rev. A **65**, 043406 (2002).
[16] M. E. Crenshaw and C. M. Bowden, Phys. Rev. Lett. **69**, 3475 (1992).
[17] Z. Lu and K. Zhu, J. Phys. B **41**, 185503 (2008).
[18] W. Zhang, A. O. Govorov, and G. W. Bryant, Phys. Rev. Lett. **97**, 146804 (2006).
[19] J. N. Farahani, D. W. Pohl, H. J. Eisler, and B. Hecht, Phys. Rev. Lett. **95**, 017402 (2005).
[20] K. T. Shimizu, W. K. Woo, B. R. Fisher, H. J. Eisler, and M. G. Bawendi, Phys. Rev. Lett. **89**, 117401 (2002).
[21] A. O. Govorov, G. W. Bryant, W. Zhang, T. Skeini, J. Lee, N. A. Kotov, J. M. Slocik, and R. R. Naik, Nano Lett. **6**, 984 (2006).
[22] R. D. Artuso and G. W. Bryant, Nano Lett. **8**, 2106 (2008).
[23] R. D. Artuso and G. W. Bryant, Phys. Rev. B **82**, 195419 (2010).
[24] D. E. Chang, A. S. Sørensen, P. R. Hemmer, and M. D. Lukin, Phys. Rev. Lett. **97**, 053002 (2006).
[25] D. E. Chang, A. S. Sørensen, P. R. Hemmer, and M. D. Lukin, Phys. Rev. B **76**, 035420 (2007).
[26] E. Chang, A. S. Sørensen, E. A. Demler, and M. D. Lukin, Nat. Phys. **3**, 807 (2007).
[27] F. Oulton, V. J. Sorger, T. Zentgraf, R. M. Ma, L. Dai, G. Bartal, and X. Zhang, Nature (London) **461**, 629 (2009).
[28] A. Manjavacas, F. J. Garcia de Abajo, and P. Nordlander, Nano Lett. **11**, 2318 (2011).
[29] A. Manjavacas, P. Nordlander, and F. J. Garcia de Abajo, ACS Nano **2**, 1724 (2012).
[30] F. H. L. Koppens, D. E. Chang, and F. J. Garcia de Abajo, Nano Lett. **11**, 3370 (2011).
[31] A. O. Govorov, G. W. Bryant, W. Zhang, T. Skeini, J. Lee, N. A. Kotov, J. M. Slocik, and R. R. Naik, Nano Lett. **6**, 984 (2006).
[32] E. Dulkeith, M. Ringler, T. A. Klar, J. Feldmann, A. Monoz, and W. J. Parak, Nano Lett. **5**, 585 (2005).
[33] S. M. Sadeghi, Nanotechnology **20**, 225401 (2009).
[34] A. V. Malyshev and V. A. Malyshev, Phys. Rev. B **84**, 035314 (2011).
[35] M. T. Cheng, S. D. Liu, and Q. Q. Wang, Appl. Phys. Lett. **92**, 162107 (2008).
[36] Q. Q. Wang, A. Muller, M. T. Cheng, H. J. Zhou, P. Bianucci, and C. K. Shih, Phys. Rev. Lett. **95**, 187404 (2005).
[37] A. O. Govorov, Phys. Rev. B **82**, 155322 (2010).
[38] P. B. Johnson and R. W. Christy, Phys. Rev. B **6**, 4370 (1972).
[39] A. Muller, Q. Q. Wang, P. Bianucci, C. K. Shih, and Q. K. Xue, Appl. Phys. Lett. **84**, 981 (2004).
[40] Q. Q. Wang, A. Muller, M. T. Cheng, H. J. Zhou, P. Bianucci, and C. K. Shih, Phys. Rev. Lett. **95**, 187404 (2005).

[41]T. H. Stievater, X. Li, D. G. Steel, D. Gammon, D. S. Katzer, D. Park, C. Piermarocchi, and L. J. Sham, Phys. Rev. Lett. **87**, 133603 (2001).
[42]A. S. Lenihan, M. V. Gurudev Dutt, D. G. Steel, S. Ghosh, and P. K. Bhattacharya, Phys. Rev. Lett. **88**, 223601 (2002).
[43]L. C. Andreani, G. Panzarini, and J. M. Gérard, Phys. Rev. B **60**, 13276 (1999).
[44]V. A. Malyshev, F. Carreño, M. A. Antón, O. G. Calderón, and F. Domínguez-Adame, J. Opt. B **5**, 313 (2003).
[45]V. A. Malyshev, I. V. Ryzhov, E. D. Trifonov, and A. I. Zaitsev, Opt. Commun. **180**, 59 (2000).
[46]A. A. Rangelov and N. V. Vitanov, Phys. Rev. A **85**, 043407 (2012).
[47]X. Yang, Y. Huang, Z. Zhang, and X. Yan, Opt. Commun. **285**, 2101 (2012).